

# Study on application of independent component analysis in the CSNS/RCS\*

AN Yu-Wen(安宇文) WANG Sheng(王生)<sup>1)</sup>

Institute of High Energy Physics, Chinese Academy of Sciences, Beijing 100049, China

**Abstract:** The China Spallation Neutron Source (CSNS) accelerators consist of a low energy  $H^-$  linac and a high energy proton Rapid Cycling Synchrotron (RCS). The proton beam is accumulated in the RCS and accelerated from 80 MeV to 1.6 GeV with a repetition of 25 Hz. Independent component analysis (ICA) is a robust method for processing the collected data (samples) recorded by the turn-by-turn beam position monitor (BPM), which was recently applied to the accelerator. The samples are decomposed to source signals, or the so-called independent components, which correspond to the inherent motion of samples, such as betatron motion and synchrotron motion. A study on the application of the ICA method to CSNS/RCS has been made. It shows that the beta function, phase advance, and dispersion can be well reconstructed by using ICA in CSNS/RCS. The effects of BPM errors on the ICA results are also studied. By comparing the different solving methods in ICA, the so-called SOBI has more advantages for isolating the independent components on the application of ICA to CSNS/RCS. Beam emittance dilution in the process of exciting the turn-by-turn samples is considered, and thus an RF kicker is adopted to avoid such emittance growth.

**Key words:** independent component analysis, turn-by-turn BPM, RF kicker

**PACS:** 28.41.ak, 41.85.Qg, 29.27.fh **DOI:** 10.1088/1674-1137/37/3/037006

## 1 Introduction

The CSNS accelerators consist of an  $H^-$  Linac and a Rapid Cycling Synchrotron (RCS). The  $H^-$  beam is accelerated to 80 MeV in the linac and then stripped to a proton beam during the injection procedure into the RCS. The proton beam is accumulated and accelerated to 1.6 GeV in the RCS, and then extracted for striking the neutron target [1]. Table 1 shows the main parameters of the RCS.

In recent years, independent component analysis has become a very popular method for blind source separation (BSS) in the fields of signal processing, medical imaging, telecommunications, etc. By isolating the underlying sources from lots of samples, ICA can obtain a great deal of useful information, and the system behavior can be better understood. The ICA method was first introduced to beam measurement in accelerators by S.Y. Lee's team [2], for treating the samples recorded by turn-by-turn BPMs. In the application of ICA to accelerators, there are two main categories. In the first one, it is assumed that the sources are non-Gaussian, and the independent component has maximum non-Gaussianity. The FastICA [3], which is based on a fixed-point iteration scheme for searching the non-Gaussianity of the source

signals, is a widely used code in this category. In the second category, it is based on the assumption that the independent components have narrow-band power spectra, and consequently the time-lag covariance matrices are diagonal. The SOBI algorithm [4] is more popular in this category due to the use of multiple time-lag covariance matrices.

Table 1. Main parameters of the RCS.

parameter	value
circumference/m	227.92
repetition rate/Hz	25
average current/ $\mu$ A	62.5
Inj. energy/MeV	80
Ext. energy/GeV	1.6
beam power/kW	100
nominal tunes (H/V)	4.86/4.78
number of BPM (H/V)	32(H)/32(V)
acceptance/ $(\pi$ mm·mrad)	540

To excite the beam for obtaining turn-by-turn BPM data, an RF kick or a pinger can be chosen. However, the beam emittance can be diluted by a pinger, so an RF kicker is chosen.

Received 15 May 2012

\* Supported by National Natural Science Foundation of China (11175193)

1) Corresponding author. E-mail: wangs@ihep.ac.cn

©2013 Chinese Physical Society and the Institute of High Energy Physics of the Chinese Academy of Sciences and the Institute of Modern Physics of the Chinese Academy of Sciences and IOP Publishing Ltd

## 2 Oscillation driven by an RF kicker

An RF kicker can excite the transverse coherent beam oscillation with a sinusoidal oscillating dipole field when its frequency is close to the betatron frequency. If the amplitude of the RF kicker field is adiabatically ramped up and down, it can produce large coherent beam oscillations. To control and preserve the particle beam emittance, a high frequency RF kicker can be slowly energized to its maximum field and likewise slowly de-energized, and the betatron oscillation can be controlled adiabatically [5]. For this feature, an RF kicker has been used in the AGS, RHIC, SPS, LHC, and Tevatron [6].

We define  $\nu_m = \omega_m / \omega_0$  as the modulation tune, where  $\omega_0$  is the orbital angular frequency, and  $\omega_m$  is the RF kicker's angular frequency. When  $n + \nu_m \approx \nu$ , the beam will be driven coherently, and the amplitude of betatron motion grows linearly with time, as shown in Eq. (1) [7]

$$y(s) \approx - \left[ \frac{\beta(s)\beta_0^{3/2}\theta_a\nu}{4\pi R} \frac{s}{R} \right] \cos \frac{\nu s}{R} + \dots, \quad (1)$$

where  $\theta_a$  is the RF kicker angle,  $\beta(s)$  and  $\beta_0$  are the beta functions in the positions of BPM and RF kicker, respectively.  $R$  is the average radius,  $s$  is the longitudinal position and  $\nu$  is the tune of the transverse motion. Fig. 1 shows the driven oscillation excited by the RF kicker. The RF kicker is switched off when the beam oscillation reaches proper amplitude, and the data of the free oscillations are stored for ICA processing. The first 200 turns are the rise time, and the latter 800 turns are free oscillation after excitation. The amplitude of the RF kicker is 0.2 mrad. The RF kicker works at a repetition rate of 449 kHz, which means  $\nu_m = 0.14$ , corresponding to the beam angular frequency of 3.212 MHz in the beam energy of 80 MeV.

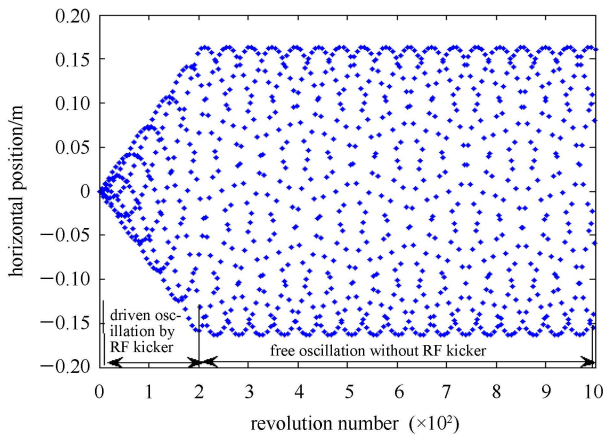


Fig. 1. Driven betatron oscillation with an RF kicker and free betatron oscillation without an RF kicker.

## 3 Reconstruction of Twiss parameters by ICA

The samples obtained from turn-by-turn BPMs can be recorded in the vector  $\mathbf{x}(t) = [x_1(t), \dots, x_m(t)]^T$ , and assumed to be generated by

$$\mathbf{x}(t) = \mathbf{A}\mathbf{s}(t), \quad (2)$$

where  $\mathbf{A} \in \mathbb{R}^{m \times n}$  is the mixing matrix with  $m \geq n$  ( $n$  is the row index of the estimated matrix).

In the first category, a linear transformation of Eq. (2) is made and the estimated sources become

$$\mathbf{y} = \mathbf{w}'\mathbf{x} = \mathbf{w}'\mathbf{A}\mathbf{s} = \mathbf{z}'\mathbf{s}. \quad (3)$$

Because the term  $\mathbf{z}'\mathbf{s}$  is more Gaussian than any of the  $s_i$  and becomes least Gaussian when it in fact equals one of the  $s_i$ , and then the estimated independent sources can be identified one by one through searching for the least non-Gaussian point. Finally the whole independent components can be written as

$$\mathbf{s} = \mathbf{A}^{-1}\mathbf{x}. \quad (4)$$

In the second category of the ICA processing, the source signals are assumed to be mutually independent and temporally correlated. Consequently, the covariance matrix  $C_s \equiv \langle \mathbf{s}(t)\mathbf{s}(t)' \rangle$  is diagonal. The samples are the linear combination of the independent components; so the covariance matrix of the samples  $C_X \equiv \langle \mathbf{X}(t)\mathbf{X}(t)' \rangle$  is not diagonal. In order to get the relationship between the independent components and the samples, the singular value decomposition (SVD) method can be used to extract the independent components from samples because the covariance matrix of the samples can be decomposed into the product of the unitary matrix and the diagonal matrix, and the diagonal matrix is just the covariance matrix of the independent components. Because the unitary matrix is not always unique in the SVD process, a proper unitary matrix needs to be figured out to be multiplied to the former unitary matrix to make the covariance matrix of the extracted independent components more diagonal. A time-lagged factor  $\tau$  is always used in the process of estimating the mixing matrix and the independent components matrix, and the sample's covariance matrix can be decomposed, as

$$C_X(\tau) = \mathbf{A}C_s(\tau)\mathbf{A}', \quad (5)$$

where  $C_X(\tau) \equiv \langle \mathbf{X}(t)\mathbf{X}(t+\tau)' \rangle$  and  $C_s(\tau) \equiv \langle \mathbf{s}(t)\mathbf{s}(t+\tau)' \rangle$  are the time-lagged covariance matrix of the samples and the independent components, respectively. Finally, the independent components  $\mathbf{s}$  and the mixing matrix  $\mathbf{A}$  can be well estimated as Eq. (6) and Eq. (7) [2],

$$\mathbf{s} = \mathbf{W}'\mathbf{V}\mathbf{X}, \quad (6)$$

$$\mathbf{A} = \mathbf{V}^{-1}\mathbf{W}, \quad (7)$$

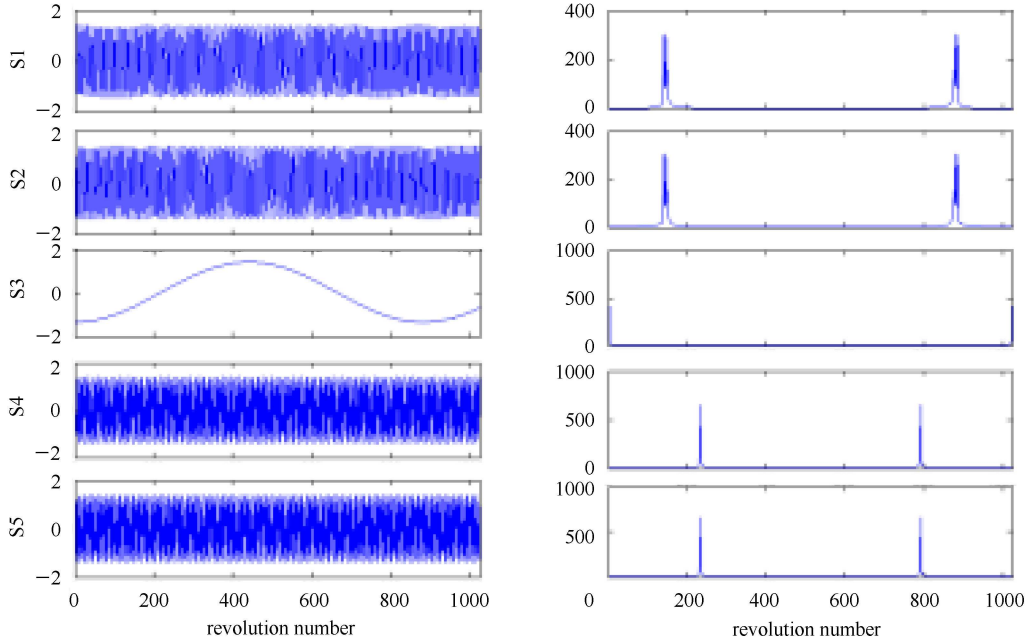


Fig. 2. The temporal function of FastICA decomposition and their spectra in the frequency domain.

where  $\mathbf{W}$  is the unitary matrix related with time-lagged factor  $\tau$ , and  $\mathbf{V} \equiv \mathbf{A}_1^{-1/2} \mathbf{U}_1'$ .  $\mathbf{A}_1$  and  $\mathbf{U}_1$  are the diagonal matrix and unitary matrix in the SVD process of the covariance matrix of samples without a time-lagged factor.

There are 32 horizontal BPMs and 32 vertical BPMs in the RCS. To get coherent betatron oscillation and synchrotron oscillation, the initial amplitudes of beam oscillation are set to 0.015 m in both horizontal and vertical directions, and the RF cavity is included in the simulation. The turn-by-turn BPM tracking data are obtained by using the Accelerator Toolbox (AT) [8]. BPMs are assumed to work perfectly and there is no noise in the samples. The independent components are obtained by using the FastICA code. The results of FastICA decomposition are shown in Fig. 2. S1 and S2 are related to the horizontal betatron oscillation; S4 and S5 are related to the vertical betatron oscillation. S3 is the synchrotron motion caused by energy variation about  $1 \times 10^{-5}$ . As an arbitrary similar permutation matrix can be multiplied to mixing matrix  $\mathbf{A}$  and estimated sources matrix  $\mathbf{S}$ , the samples matrix  $\mathbf{X}$  does not change. Therefore, the order of estimated sources cannot be directly determined by FastICA, and with the help of the mode frequency, the modes can be distinguished.

### 3.1 Betatron function and phase advance calculated from the spatial function

In the FastICA process, betatron functions and phase advance can be derived from Eq. (4)

$$\beta = a(A_{s1}^2 + A_{s2}^2), \quad \varphi = \tan^{-1}(A_{s1}/A_{s2}). \quad (8)$$

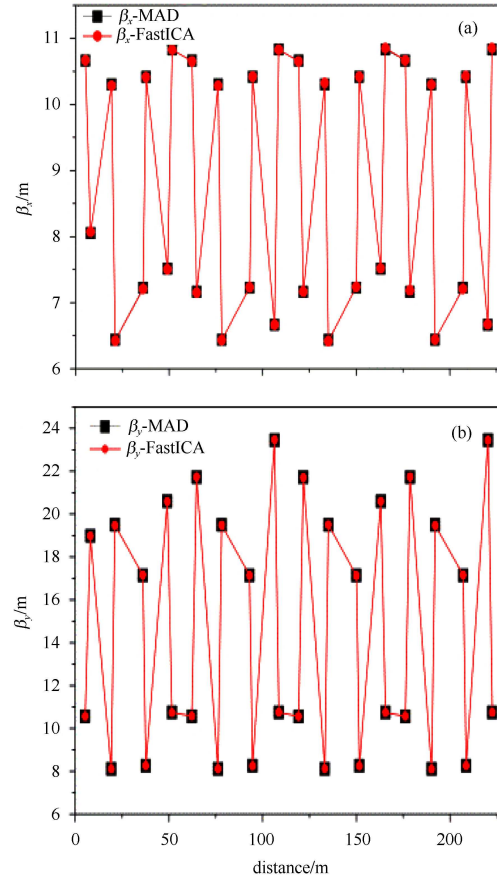


Fig. 3. Beta function comparison between FastICA and theoretical value. (a) The horizontal beta function comparison. (b) The vertical beta function comparison.

The numbers and positions of the BPM in the RCS are not important for the FastICA algorithm. Generally, BPMs are often located near the quadruples, and they can reflect the beta beating. The constant  $a$  equals  $2J$  ( $J$  is the action of the Hamiltonian system) in a linear conservative system, and can be scaled from the model

$$\sum_{i=1}^M \frac{1}{\beta_{i,ICA}} = \sum_{i=1}^M \frac{1}{\beta_{i,MAD}}, \quad (9)$$

where  $M$  is the number of the BPM. Fig. 3 shows the beta function calculated by FastICA and that from MAD. It shows that the results agree well with the theoretical model.

Actually, the phase advance can be calculated accurately from Eq. (8) between two adjacent BPMs. However, the initial phase in the first BPM also needs to be calibrated with the theoretical model. Fig. 4 shows the phase advance comparison between FastICA and the theoretical values. The results agree well with each other.

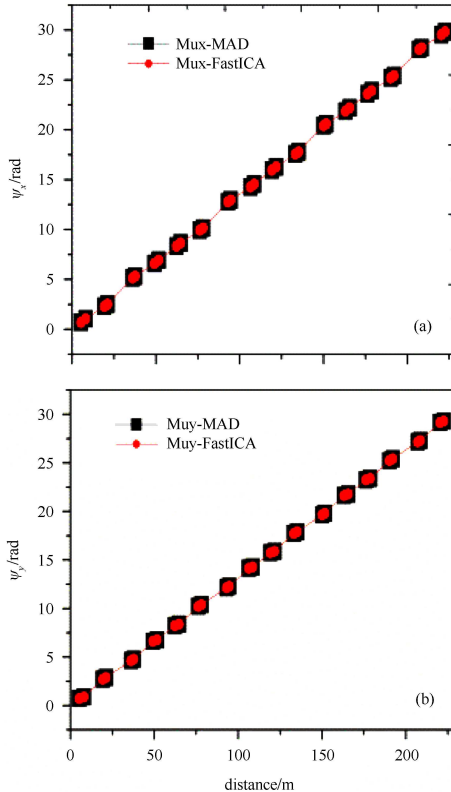


Fig. 4. Phase advance comparison between FastICA and theoretical value. (a) The horizontal phase advance comparison. (b) The vertical phase advance comparison.

### 3.2 Synchrotron motion

Component S3 in Fig. 2 represents the synchrotron motion, and is related to the horizontal dispersion func-

tion and momentum deviation. The relationship between the dispersion function and the momentum deviation can be written as

$$\Delta p/p(s,t) = \frac{1}{D(s)} A_s(s) s_s(t), \quad (10)$$

where  $s_s(t)$  represents the synchrotron component and  $A_s$  the corresponding mixing vector. From Eq. (10), one can easily get

$$\Delta p/p(s,t) = \frac{1}{b} s_s(t), \quad (11)$$

$$D(s) = b A_s(s). \quad (12)$$

The constant  $b$  can be scaled by the theoretical model.

Figure 5 shows the dispersion function obtained with ICA and the comparison with the theoretical model. The ICA results agree well with the theoretical model.

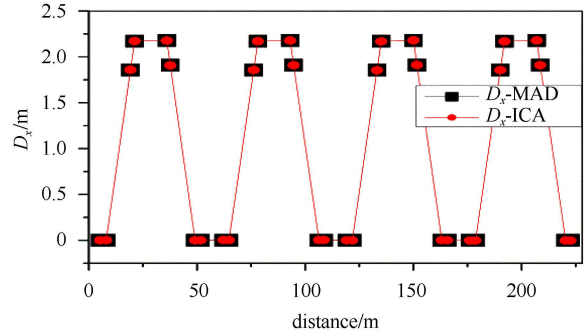


Fig. 5. Dispersion function comparison between FastICA and the theoretical value.

## 4 The effects of errors on the ICA results

In case of decomposition of the perfect data without error, it is good enough to find the independent components accurately. However, for a real machine, the data of BPMs always include errors, and these errors become white noise in the ICA simulation. For CSNS/RCS, due to the large aperture of the vacuum chamber, the errors of BPM can be as large as 1 mm.

In the simulation with data including errors, both the horizontal and vertical BPM turn-by-turn data are recorded into matrices, with an error of 0.4 mm. The introduced errors follow the uniform distribution, and the RF cavity is turned off. The amplitudes of beam oscillation are set to 0.015 m in both the horizontal and vertical directions. The errors of decomposed components due to the error introduced in the BPM data are in Fig. 6, in which the errors are defined as rms differences between the theoretical model and the values obtained from ICA.

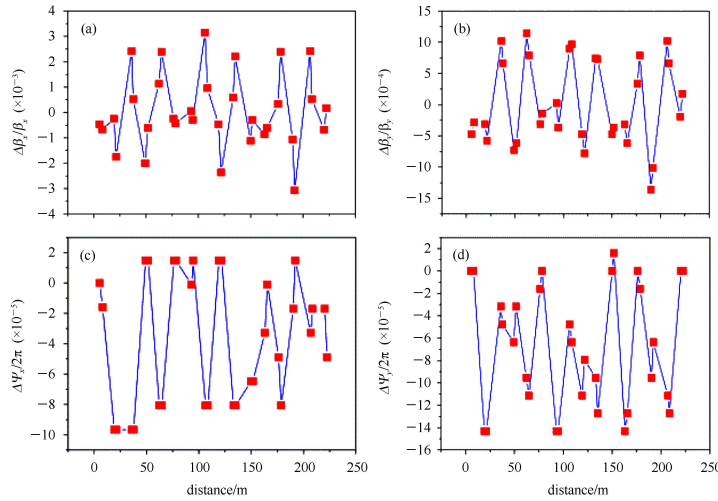


Fig. 6. The ICA errors due to the noise of 0.4 mm. (a) The horizontal beta-beating between SOBI and the theoretical values. (b) The vertical beta-beating between SOBI and theoretical values. (c) The normalized horizontal phase advance differences between SOBI and theoretical values. (d) The normalized vertical phase advance differences between SOBI and theoretical values.

In the noise level of around 0.4 mm, the ICA decomposition can be done well by using FastICA. But with the increase of the noise, the betatron function cannot be isolated. The two main reasons may be speculated as follows. One is that the non-Gaussianity should be measured in a very accurately model. The classical measurement of the non-Gaussianity is kurtosis or the fourth-order cumulant, and can be defined by  $kurt(s) = E\{s^4\} - 3(E\{y^2\})^2$ . Because kurtosis is very sensitive to the outliers, and its value may depend on only a few observations in the tails of the distribution, it is not a robustness measure of non-Gaussianity. Negentropy, which is based on the information quantity of the (differential) entropy, is a second important measure of non-Gaussianity. However, the estimation of negentropy is always difficult, and some approximation has to be used, and then the inaccuracy will be brought about. The other reason is that the least non-Gaussian point found by the FastICA algorithm is not always the global maximum point. By using the Newton method, the maximum non-Gaussian point found in the gradient direction is always the local maximum point.

To deal with data with large noise, another ICA code, SOBI, is used. As stated from Eq. (5) to Eq. (7), the independent sources are estimated by decomposing the time-lag covariance of the samples. In the SOBI algorithm, the samples recorded from turn-by-turn BPMs are whitened to make the covariance of the samples form an identity matrix and facilitate to next step. Because the covariance of the independent sources is identical, the SVD of the time-lag covariance of the whitened samples can improve the estimated independent sources accuracy. By using SOBI, the betatron motions can be well

isolated even with large noise, especially in the case of many independent sources mixed together. Fig. 7 shows the betatron isolation errors by using FastICA and SOBI respectively. When the BPM noise level reaches 900  $\mu\text{m}$ , the FastICA cannot extract the independent components from samples, and a pink (blue) up-down line appears at 800  $\mu\text{m}$ .

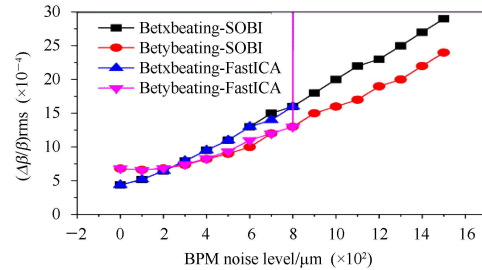


Fig. 7. The errors of beta function vs. BPM noise levels isolated by using FastICA and SOBI.

To decompose the dispersion, the RF cavity is turned on. The noise just added to the horizontal samples and the noise level is around 1 mm. After the FastICA algorithm process, five synchrotron signals emerged and no synchrotron component matched the energy variation. The sum of any two or three of the total five synchrotron components also fails to match the energy variation. By using SOBI, the synchrotron motion is unique, and the corresponding mixed vector of that signal represents the dispersion function. If an initial 80 keV energy kick is put to the RF cavity, the FastICA can also isolate synchrotron motion. Fig. 8 shows the dispersion function isolated by using the FastICA and SOBI, with the noise included.

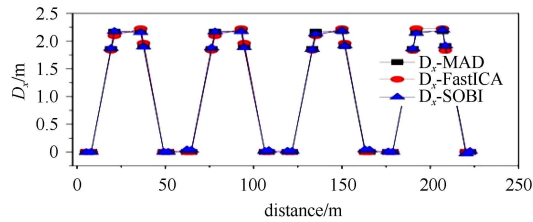


Fig. 8. The dispersion function decomposed by FastICA and SOBI.

With large noise, the dispersion function can be decomposed by both FastICA and SOBI. However, for FastICA, the beam needs to be strongly excited in synchrotron motion, and this is difficult in the operation of the RCS. The reason should be that the synchrotron motion is weak, though the noise level is high. Synchrotron motion cannot be estimated by putting linear transformation to samples to get the least non-Gaussian point of the synchrotron motion. By using SOBI, the dispersion function can be decomposed without the strong excitation of synchrotron motion.

## 5 ICA detection of a malfunctioning BPM

To further illustrate the robustness of ICA, a narrow-band bad-BPM harmonic oscillation has a ripple noise, with the level of 1 mm and a frequency of 0.84, which is very close to the betatron frequencies. In the simulation, the other noises of BPMs are set to the level of 1 mm. The RF cavity is supposed to match the magnetic field, so there is no synchrotron independent component in the ICA process. By using SOBI, the mode corresponding to the ripple noise of the malfunction is successfully isolated. As shown in Fig. 9, the mode S5 corresponds to the ripple noise, while S1 and S2 represent the vertical independent components, and S3 and S4 represent the horizontal independent components. By using ICA, the malfunction BPM is detected, even though the frequency of the ripple noise is very close to the horizontal tune of the beam. As the mode of the malfunction BPM is separated, the other two transverse modes can be well isolated, and thus the horizontal and vertical beta functions and phase advance can be calculated accurately.

The RMS error of the beta function obtained from the ICA and the theoretical model is 0.003 and 0.0025 for the horizontal and vertical planes respectively, and the horizontal and vertical phase advances are 0.00032 and 0.00035, respectively.

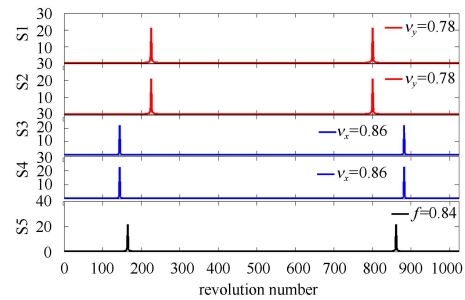


Fig. 9. The spectra of S1-S5 modes in the frequency domain.

## 6 Summary and discussion

The study of the application of ICA on the CSNS/RCS was done for decomposing the Twiss parameters. The two widely used categories of ICA are in the field of blind source separation and were introduced and applied to the CSNS/RCS. The Twiss parameters can be well decomposed based on the turn-by-turn BPM data, even in the existence of large noise in the BPM data. By comparing the applications of the two categories in the CSNS/RCS, it is found that FastICA is appropriate for the strong signal and the noise level should be strictly controlled. The SOBI is more robust for noise and more powerful to extract very weak signals, but it requires that the signal spectrum be narrowband and not overlapping with each other. In the CSNS/RCS case, the separation among the modes can meet the requirement of SOBI, so SOBI will be adopted in the CSNS/RCS commissioning. In the simulation study, magnet errors were not introduced to the CSNS/RCS lattice, so the Twiss parameters obtained from ICA are very close to the theoretical value. The ICA application on CSNS/RCS with magnet errors will be done in our future study.

*We wish to thank Professor Lee S Y for his helpful suggestions and useful discussions on ICA application.*

## References

- 1 WANG S, AN Y W, FANG S X et al. Scientific China Physics Mechanics & Astronomy, 2011, **54**(Suppl 2): s239-s224
- 2 HUANG X, Lee S Y, Prebys E, Tomlin R. Phys. Rev. ST Accel. Beams, 2005, **8**: 064001
- 3 Hyvarinen A, Oja E. Independent Component Analysis: Algorithms and Applications. Helsinki University of Technology, Finland. 2000
- 4 Belouchrani A, Abed-Merain K, Cardoso J F, Moulines E. IEEE Trans. Signal Processing, 1997, **45**: 434-444
- 5 BAI M, Lee S Y, Glenn J W, HUANG H, Ratner L, Roser T, Sypher M J, van Asselt W. Phys. Rev. E, 1997, **56**: 6002
- 6 Miyamoto R, Kopp S E. Phys. Rev. ST Accel. Beams, 2008, **11**: 084002
- 7 Lee S Y. Accelerator Physics. 2<sup>nd</sup> ed. Singapore: World Scientific, 2004
- 8 <http://www.slac.stanford.edu/grp/ssrl/spear/at/>